Performance improvement of CdS/Cu(In,Ga)Se_2 solar cells after rapid thermal annealing*

Chen Dong-Sheng(陈东生)[a)b)], Yang Jie(杨 洁)[a)], Xu Fei(徐 飞)[a)], Zhou Ping-Hua(周平华)[a)], Du Hui-Wei(杜汇伟)[a)], Shi Jian-Wei(石建伟)[a)], Yu Zheng-Shan(于征汕)[c)], Zhang Yu-Hong(张玉红)[c)], Brian Bartholomeusz[d)], and Ma Zhong-Quan(马忠权)[a)†]

[a)] *SHU-SolarE R & D Laboratory, Department of Physics, Shanghai University, Shanghai* 200444, *China*
[b)] *College of Mathematics and Physics, Shanghai University of Electric Power, Shanghai* 200090, *China*
[c)] *Shanghai Solar EnerTech Co. Ltd, Shanghai* 201206, *China*
[d)] *Applied Quantum Technology Ltd. Co. USA*

(Received 27 April 2012; revised manuscript received 15 July 2012)

In this paper, we investigated the effect of rapid thermal annealing (RTA) on solar cell performance. An opto-electric conversion efficiency of 11.75% ($V_{oc} = 0.64$ V, $J_{sc} = 25.88$ mA/cm^2, FF=72.08%) was obtained under AM 1.5G when the cell was annealed at 300 °C for 30 s. The annealed solar cell showed an average absolute efficiency 1.5% higher than that of the as-deposited one. For the microstructure analysis and the physical phase confirmation, X-ray diffraction (XRD), Raman spectra, front surface reflection (FSR), internal quantum efficiency (IQE), and X-ray photoelectron spectroscopy (XPS) were respectively applied to distinguish the causes inducing the efficiency variation. All experimental results implied that the RTA eliminated recombination centers at the p–n junction, reduced the surface optical losses, enhanced the blue response of the CdS buffer layer, and improved the ohmic contact between Mo and Cu(In, Ga)Se_2 (CIGS) layers. This leaded to the improved performance of CIGS solar cell.

Keywords: CdS/Cu(In,Ga)Se_2, solar cell, rapid thermal annealing, performance improvement

PACS: 88.40.jn, 68.35.–p **DOI:** 10.1088/1674-1056/22/1/018801

1. Introduction

Polycrystalline Cu(In,Ga)Se_2 (CIGS) is one of the most promising materials for thin-film solar cells due to its low consumption of materials, long term durability, stability, and high conversion efficiency. The recorded efficiency is beyond 20%, the highest for polycrystalline thin film devices.[1] During the fabrication of solar cells, annealing is a very important step because it can effectively eliminate the defect compounds in the thin films, activate the doping impurities in the bulk, and improve the ohmic contact at the interfacial region.[2,3] However, the conventional furnace heating has a high thermal budget, long cycle time, and temperature non-uniformity for large-diameter wafers, which can lead to the doping impurity diffusion. Rapid thermal annealing (RTA) not only offsets the disadvantages of conventional furnace heating but also precisely controls the annealing profile. Therefore, the RTA treatment has become a very popular thermal processing method in recent years.

Nowadays, the technique has been widely used for the post-treatment processing of CIGS thin film in order to minimize damage and eliminate defect compounds in the thin film. Miyazaki *et al*. used the RTA treatment to remove the $Cu_{2-x}Se$ compound on a CIGS thin film surface. The efficiency of the cell had about 3.9% absolute improvement from 7.3% to 11.2% when the annealed thin film was fabricated into a solar cell. The performance improvement was attributed to the reduction of recombination at the CdS/CIGS interface.[4] Chung *et al*. found that the optical transmittance of CdS thin film had a slight increase at short wavelength after annealing. The efficiency of the cell had about 0.6% absolute improvement from 15.87% to 16.47% when the annealed CdS/CIGS thin film was fabricated into a solar cell.[5] Meanwhile, the technique has also been used for the post-treatment of solar cells. Wang *et al.* studied the effects of defect density on the cell performance by fitting the experimental data of RTA-treated CIGS cells using the AMPS-1D device simulation program.[6] Though it is clear that the efficiency can be remarkably improved after annealing, the physical mechanisms are still unclear and need to be clarified.

In this paper, an efficiency improvement of CIGS solar cells is reported by using the RTA treatment. Meanwhile, we investigate the effect of RTA treatment on defect compounds in the CIGS absorber layer, the square resistance, the surface reflection of the windows layer, and the Mo/CIGS interfacial ohmic contact respectively.

*Project supported by the National Natural Science Foundation of China (Grant No. 60876045), the Shanghai Leading Basic Research Project, China (Grant No. 09JC1405900), the Shanghai Leading Academic Discipline Project, China (Grant No. S30105), and the R & D Foundation of SHU-SOENs PV Joint Laboratory, China (Grant No. SS-E0700601).

†Corresponding author. E-mail: zqma@shu.edu.cn

© 2013 Chinese Physical Society and IOP Publishing Ltd

2. Experiment

2.1. Fabrication procedures of solar cells

An Mo layer of about 1000 nm thickness was first deposited on SLG substrates as the back contact layer by direct-current magnetron sputtering. Then, a CIGS absorber layer with a thickness of 1200 nm was grown by two step-sputtering techniques.[7] A CdS buffer layer with a thickness of 50 nm was fabricated by chemical bath deposition (CBD) using $CdSO_4$ (0.0015 M), NH_4OH (1.5 M), and thiourea (0.05 M) aqueous solution at approximately 70 °C. After that, about 100 nm i-ZnO layer and 550 nm thick AZO windows layer were prepared by magnetron sputtering respectively. Finally, a patterned metal grid (Ni/Al) was deposited by vacuum evaporation.

2.2. Annealing process

After the front electrodes were fabricated, the cells were moved into a rapid thermal processing (RTP) furnace and heated by tungsten halogen lamp arrays. The process was performed in ambient N_2. In order to study the impact of RTA on the CIGS device, the cells were orderly annealed at different temperatures (100 °C, 150 °C, 300 °C, 400 °C, 500 °C) for 30 s. After each annealing, the cells were examined using a solar simulator (AM 1.5G, 100 mW/cm^2). The annealing temperature curves were divided into three parts, as shown in Fig. 1. In the first part (I), the temperature was raised from room temperature to a different annealing temperature, the rate of heating-up was 50 °/s. In the second part (II), the temperature was held at the annealing temperature for 30 s. In the third part (III), the temperature was dropped to room temperature with natural cooling under a low vacuum of about 2.0 Pa.

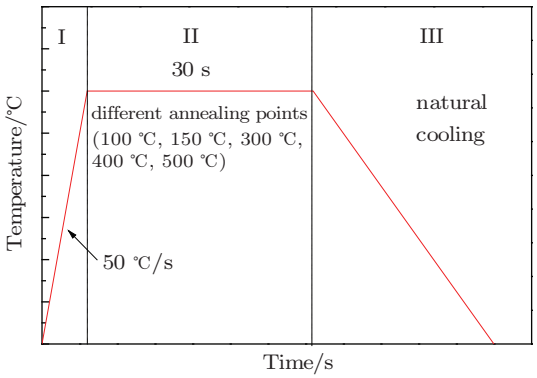


Fig. 1. (color online) Annealing temperature curves of CIGS solar cells.

3. Results and discussion

3.1. Results

Some important electrical parameters of CIGS solar cells obtained after different annealings are shown in Table 1. As can be seen, the short-circuit current densities (J_{sc}) and the filled factors (FF) have remarkable improvements when the annealing temperature is lower than 300 °C. The significant improvements of J_{sc} and FF are mainly responsible for the increase of the efficiency of solar cells, because V_{oc} basically is kept a constant. Unfortunately, V_{oc} and FF both become worse after annealing at 500 °C, indicting the microstructure of the device has been destroyed. All J–V curves are shown in Fig. 2.

Table 1. The J–V characteristics of CIGS solar cells obtained after different annealings.

Annealing conditions	V_{oc}/V	J_{sc}/mA·cm^{-2}	FF/%	Efficiency/%
without annealing	0.64	23.20	68.86	10.22
100 °C, 30 s,	0.63	23.17	69.87	10.20
150 °C , 30 s	0.63	23.71	71.58	10.69
300 °C , 30 s,	0.63	25.88	72.08	11.75
400 °C, 30 s	0.60	26.20	64.82	10.19
500 °C, 30 s,	0.36	26.64	36.91	3.54

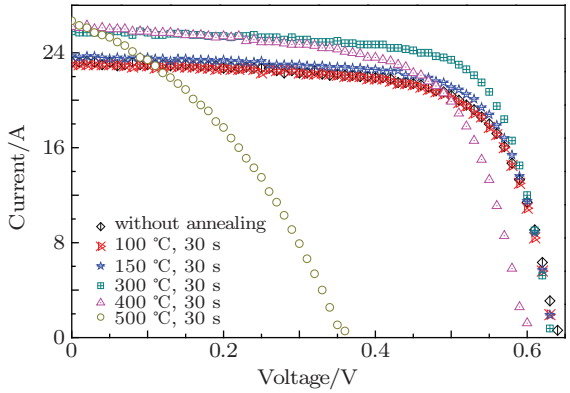


Fig. 2. (color online) The J–V curves of CIGS solar cells.

We extract the series resistance R_s and the parallel resistance R_{sh} from the light current–voltage curves. When the annealing temperature reaches 300 °C, R_s drops from 0.52 Ω to 0.35 Ω and R_{sh} raises from 130.89 Ω to 411.52 Ω. Meanwhile, the FF also reaches the maximum value.

The above experiment results show that 300 °C is a perfect annealing temperature. So, we mainly focus on the change between the samples without any treatment and annealed at 300 °C.

3.2. Discussion

Figure 3 presents two XRD spectra that correspond to CIGS solar cells without annealing and annealed at 300 °C. The peaks indeed indicate the three main phases of crystal structure. The peaks denoted as (112), (220), and (204) can be attributed to CIGS (PDF: 35-1102), the peak denoted as (002) is attributed to ZnO (PDF: 36-1451), and the peak denoted as (110) comes from Mo (PDF: 42-1120). After annealing, the diffraction spectrum of the three main crystal structures remains unchanged. The spectral peak at approximately $2\theta = 36.4°$ corresponds to the (104) diffraction of $MoSe_2$

(PDF: 20-0757). After annealing, the diffraction spectrum of $MoSe_2$ compound becomes slightly stronger, indicating the (104) direction of polycrystalline $MoSe_2$ grows well. Additionally, the small peak located at the shoulder of the CIGS (112) peak is consistent with the (221) diffraction of $Cu_{2-x}Se$ (PDF: 06-0680) in the pristine film. It is well known that copper selenide (CuSe) formed by copper-rich CIGS is an excellent medium for enhancing the growth of grains on CIGS absorbers. However, the copper selenide cannot be exhausted during the grain growth of CIGS due to the imprecise controlling. The degradation caused by residual $Cu_{2-x}Se$ is a serious problem, which is more obvious in sputtering during selenization.

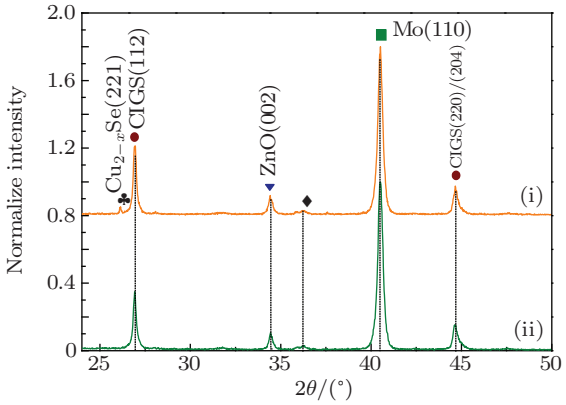


Fig. 3. (color online) XRD patterns of CIGS solar cells (i) without annealing and (ii) annealed at 300 °C.

The residual $Cu_{2-x}Se$ exists not only on the surface but also at the grain boundary. The recombination at grain boundaries is deduced to be the main loss mechanism in CdS/CIGS solar cells. The peak of $Cu_{2-x}Se$ will disappear when the cells are annealed at 300 °C, indicating that the films have been transformed from copper-poor to copper-rich films. On one hand, the removal of $Cu_{2-x}Se$ existing on the surface of CIGS eliminates recombination centers at the p–n junction. Therefore, the electron–hole pairs generated in the CdS are collected properly. This can lead to the advancing of short circuit current density of the CIGS solar cell. On the other hand, residual $Cu_{2-x}Se$ is responsible for the reverse leakage, because it produces serious pinhole defects. The removal of the residual $Cu_{2-x}Se$ between grain boundaries would improve the shunt resistance.[8] Therefore, the performance improvement of cells is deduced to be due to the decrease of recombination centers and the elimination of shunt paths.

Typical Raman spectra of CIGS thin film prepared at various annealing temperatures are shown in Fig. 4. The Raman spectra shows A1 mode at approximately 173.8 cm^{-1}, which is generally observed in I–II–VI2 chalcopyrite compounds. The as-deposited thin film has a poor structural quality. With the increase of annealing temperature the intensity of 173.8 cm^{-1} peak becomes stronger. The intensity of the Raman peak strongly depends on the phase composition in the CIGS thin film.[9] So, it is found that the RTA can enhance the crystallization of the CIGS thin film.

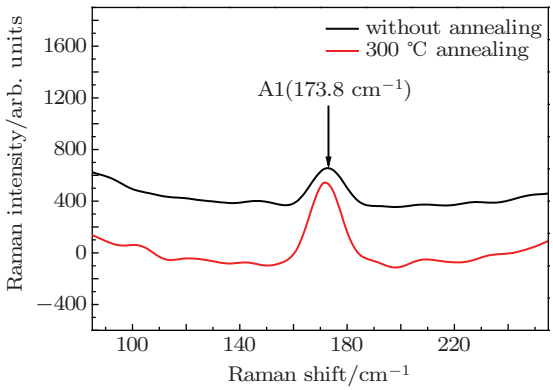


Fig. 4. (color online) Raman spectra of CIGS absorbers.

Front surface reflection (FSR) mainly comes from the air/AZO/ZnO/CdS/Cu(In,Ga)Se_2 interfaces. Figure 5 shows a plot of optical reflection versus wavelength for the TCO layer without annealing and with 300 °C annealing. All of the films exhibit low average reflection of 3–6% in the wavelength range from 400 nm to 1000 nm. Typically, there is 1–5% absorption for the TCO layer through the visible wavelengths, which increases in the near infrared region ($>$ 900 nm) due to the free carrier absorption and at short wavelengths ($<$ 400 nm) approaching the TCO band gap. Furthermore, the FSR in the wavelength range from 450 nm to 850 nm has a sharp decrease after annealing at 300 °C. Therefore, it is found that the RTA can reduce the reflection and improve the transmission of the TCO layer. That is to say, the RTA can reduce the optical loss which primarily limits the generation of carriers, contributing to improving J_{sc} of the solar cell. For high-efficiency devices, this is often minimized with an anti-reflection layer.

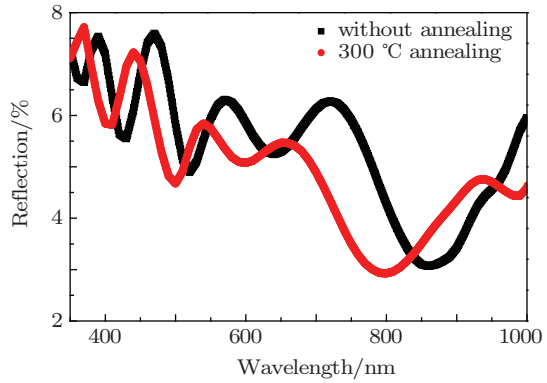


Fig. 5. (color online) Front surface reflection of CIGS solar cells.

Internal quantum efficiency (IQE) measurements are usually used to determine optical losses and optical enhancements. The IQEs of CIGS solar cells without annealing and

with 300 °C annealing are shown in Fig. 6, which can be divided into three parts based on the band gap of different layers. Parts I, II, and III correspond to ZnO, CdS, and CIGS absorber spectra, respectively. The IQE of cells is slightly increased at part II (390–520 nm) after annealing. Apparently, the RTA treatment has a positive effect on the blue response of the CdS buffer layer. For IQE, the effect of CdS becomes appreciable at wavelengths below ∼ 520 nm corresponding to the CdS band gap of 2.42 eV.[10] The reduction of optical losses shown in Fig. 6 and the removal of $Cu_{2-x}Se$ existing on the CIGS surface affect the IQE.

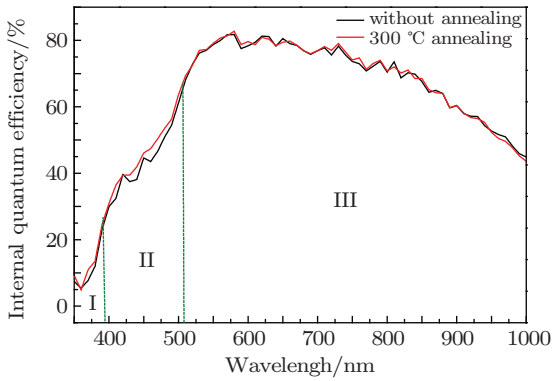


Fig. 6. (color online) Internal quantum efficiencies of CIGS solar cells.

For solar cells, some parasitic losses, such as series resistance, primarily impact the fill factor. In order to study the effect of RTA on the series resistance, the mapping of surface sheet resistance is shown in Fig. 7. The result implies that the sheet resistance of the surface layer does not remarkably change after annealing. It was reported that the resistance of the AZO films increased, while both the mobility and the carrier concentration decreased after 300 °C annealing for 30 min in air or nitrogen. The change of resistance of the AZO films mainly originated from the changes in the concentration of oxygen vacancies and adsorbed oxygen at the grain boundaries.[11] However, we do not find such a phenomenon in our study. One possible reason is that the short annealing time does not affect the concentration of oxygen vacancies and adsorbed oxygen at the grain boundaries.

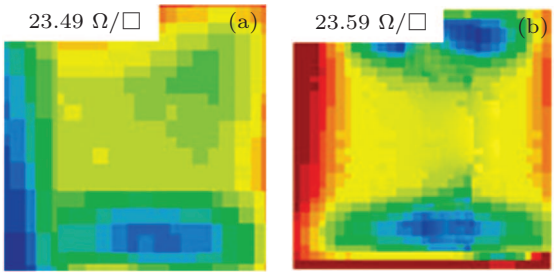


Fig. 7. (color online) Sheet resistances of CIGS solar cells (a) without annealing and (b) annealed at 300 °C.

An XPS (X-ray photoelectron spectroscopy) depth profile of Se and Mo is demonstrated in Fig. 8(a). The Se intensity varies from around 44% atomic counts to background level. A clear peak of Se is observed at the Mo/CIGS interface. The maximum peak intensity exceeds 48% atomic counts, which implies that Se-rich compounds may exist at the Mo/CIGS interface.

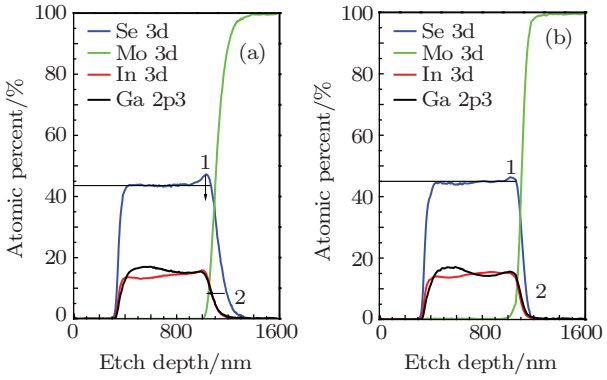


Fig. 8. (color online) XPS depth profiles of CIGS solar cells (a) without annealing and (b) annealed at 300 °C.

For the CIGS solar cell, the Mo/CIGS interfacial contact is very important. Usually, an $MoSe_2$ interfacial layer between Mo and CIGS layers is expected to reduce the interfacial contact resistance. The Mo/CIGS contact with an $MoSe_2$ layer is not of the Schottky type, but is a favorable ohmic-type contact.[12] When CIGS is grown on Mo, an interfacial layer of $MoSe_2$ is automatically formed and helps in the ohmic transport between CIGS and Mo layers. An $MoSe_2$ layer with a thickness of 150 nm was observed at the Mo/CIGS interface in a three-stage high efficiency CIGS solar cell.[13] In our cells, there exists a transitive layer between Mo and CIGS layers (cross sectional SEM image not shown). About 140 nm thickness transitive layer with columnar structures is manifested at the Mo /CIGS interface.

Meanwhile, a large number of Mo atoms move into the CIGS layer through the Mo/CIGS interface. With the help of excess Se, Mo–Se compounds ($MoSe_2$, Mo_3Se_4) of different thicknesses can be formed.[13,14] Furthermore, the $MoSe_2$ polycrystalline phase has been observed in XRD, hinting at the existence of $MoSe_2$ compound in the transitive layer.

As can be seen in Fig. 8, we also find that the interface between Mo and CIGS layers for the sample after annealing is narrower than that without annealing. The fact is that the selenide diffuses into the CIGS layer from the back contact, contributing to the swarm of $MoSe_2$ compound. This is consistent with the stronger $MoSe_2$ peak in the XRD of the annealed sample. After annealing, the interface between Mo and CIGS layers becomes clear. A clear interfacial layer with $MoSe_2$ compound can not only reduce the series resistance of the CIGS device but also improve the adhesion at the Mo/CIGS interface.

4. Conclusion

The effect of RTA on the binary compound in CIGS thin film, the optical transmittance of buffer layer CdS, the contact resistance at Mo/CIGS interface, and the cell performance of CIGS solar cells have been systematically investigated. We find that J_{sc} can mainly be attributed to the reduction of recombination centers at the p–n junction, the improvement of irradiated light intensity, and optical absorber of the buffer layer at short wavelengths in the range from 400 nm to 520 nm. The reduced R_s mainly originates from the swarm of $MoSe_2$ compound at the Mo/CIGS interface. The removal of $Cu_{2-x}Se$ compound is responsible for the advancing of R_{sh}. Correspondingly, the FF can also be improved due to the changes of R_s and R_{sh}.

Acknowledgement

Part measurement was supported by Analysis and Testing Center of Shanghai University, China.

References

[1] Green M A, Emery K, Hishikawa Y and Warta W 2011 *Prog. Photovolt. Res. Appl.* **19** 84
[2] Xu S J, Wang X C and Chua S J 1998 *Appl. Phys. Lett.* **72** 3335
[3] Liu X M, Li B C and Huang Q P 2010 *Chin. Phys.* B **19** 097201
[4] Miyazaki H, Mikami R, Yamada A and Konagai M 2004 *Jpn. J. Appl. Phys.* **43** 4244
[5] Chung Y D, Cho D H, Park N M, Lee K S and Kim J 2011 *Curr. Appl. Phys.* **11** S65
[6] Wang X, Li S S, Kim W K, Yoon S, Craciun V, Howard J M, Easwaran S, Manasreh O, Crisalle O D and Andersonb T J 2006 *Sol. Energ. Mat. Sol.* C **90** 2855
[7] Hsu H R, Hsu S C and Liu Y S 2012 *Sol. Energy* **86** 48
[8] Hsieh T P, Chuang C C, Wu C S, Chang J C, Guo J W and Chen W C 2011 *Solid. State. Electron.* **56** 175
[9] Zaretskaya E P, Gremenok V F, Riede V, Schmitz W, Bente K, Zalesski V B and Ermakov O V 2003 *J. Phys. Chem. Solids* **64** 1989
[10] Steven S H and William N S 2004 *Prog. Photovolt. Res. Appl.* **12** 155
[11] Tong H, Deng Z H, Liu Z G, Huang C G, Huang J Q, Lan H, Wang C and Cao Y G 2011 *Appl. Surf. Sci.* **257** 4906
[12] Assmann L, Berne'de J C, Drici A, Amory C, Halgand E and Morsli M 2005 *Appl. Surf. Sci.* **246** 159
[13] Wada T, Kohara N, Nishiwaki S and Negami T 2001 *Thin Solid Film.* **387** 118
[14] Guillemoles J F, Kronik L, Cahen D, Rau U, Jasenek A and Schock H W 2000 *J. Phys. Chem.* B **104** 4849